Article ID: 1000-5773(2006)01-0067-012

Dynamic Cylindrical Cavity Expansion Model and Its Application to Penetration Problems*

H. Zhou, H. M. Wen

(*Laboratory for Mechanical Behaviour and Design of Materials, University of Science and Technology of China, Hefei* 230027, *China*)

Abstract: Dynamic cylindrical cavity expansion model and its application to penetration problems were studied. Both incompressible and compressible bilinear strain-hardening material models were considered. First, solutions for dynamic cylindrical cavity expansion (DCCE) are obtained in terms of the velocity of plastic wave front, radial stress distribution and stress on the cavity surface. The influence of material properties such as compressibility, elastic-plastic constitutive equations and plastic modulus is discussed. Based on the DCCE models, penetration equations are then constructed. Comparison with experimental penetration data shows reasonable agreement between theory and experiment. It also shows that material properties such as plastic modulus have considerable effects on the dynamics cavity expansion and its resistance to penetration.

Key words: dynamic cylindrical cavity expansion; bilinear strain-hardening materials; material properties; depth of penetration

CLC number: O385 **Document code**: A

1 Introduction

An understanding of the response of structures subjected to intense dynamic loadings which produce large plastic deformation and failure are of great significance for safety calculations and assessment in a variety of engineering such as aerospace, transportation, naval architecture, chemical, nuclear and defense industry. In particular, the penetration and perforation of targets are very important for protective engineering.

Cavity expansion approximations are often used to simplify the target analyses and to formulate penetration models. While quasi-static analyses have been used for deep-punching problems in elastic-plastic materials by Bishop et al. [1], Wright et al. [2], and Satapathy et al. [3], dynamic analyses have also been developed in literatures of Goodier[4], Forrestal[5], Luk et al. [6], Luk et al. [7], and Forrestal et al. [8] etc.

Previous models for the dynamic expansion of cylindrical cavities assumed materials as either perfectly plastic[9-10] or power law strain-hardening[7] materials. However, it has been observed experimentally that most ductile materials show elastic, linear plastic hardening behavior in the true stress-true strain relationship both in tension and compression. A linear plastic hardening material model is probably more suitable for large deformation problems such as penetration and perforation of ductile targets.

The objectives of the paper are two folds. First, a theoretical study is conducted on the dynamic cylindrical cavity expansion (CSCE) from zero radius for bilinear strain-hardening material. Then, the

* **Received date**: 2004-12-06; **Revised date**: 2005-01-18
Corresponding author: H. M. Wen, professor. E-mail: hmwen@ustc.edu.cn

CSCE is employed to derive equations for penetration. Comparison of the present models with available experimental data and existing power law model is made. The influence of materials properties such as compressibility, plastic hardening modulus and elastic-plastic constitutive equations, on the CSCE and penetration is discussed.

2 Cavity Expansion Models

Cylindrical cavity expansion model assumes the target response is one-dimensional axisymmetric and only radial motion is allowed. A cylindrical symmetric cavity is expanded from zero initial radius at constant velocity v_c, as shown in Fig. 1. This expansion produces plastic and elastic response regions. The plastic response region is bounded by the radii $r=v_c t$ and $r=ct$, where r is the radial, Eulerian coordinate, t is the time, and c is the elastic-plastic interface velocity. For the compressible model the elastic region is bounded by $r=ct$ and $r=c_d t$, where c_d is the elastic dilatational velocity. For the incompressible model, there is no elastic wave front, and the elastic region occupies $r>ct$.

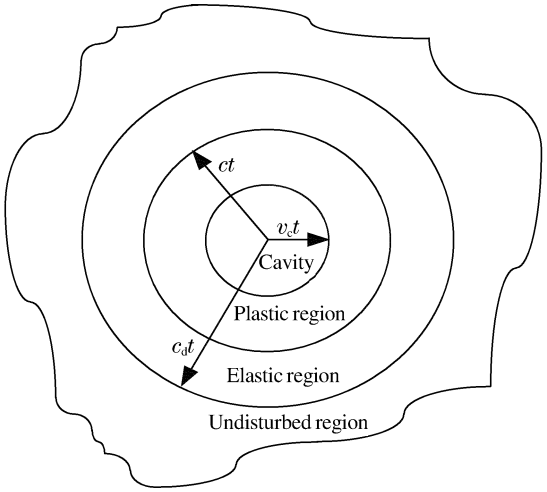


Fig. 1 Response regions

2.1 Control Equations in Plastic Region

From the momentum and mass conservation equations in Eulerian coordinates with spherical symmetry, one obtains

$$\frac{\partial \sigma_r}{\partial r}+\frac{\sigma_r-\sigma_\theta}{r}=-\rho\left(\frac{\partial v}{\partial t}+v\frac{\partial v}{\partial r}\right) \tag{1a}$$

$$\rho_0\left[\frac{\partial}{\partial r}(r-u)^2\right]=2\rho r \tag{1b}$$

where σ_r, σ_θ are the radial and hoop components of Cauchy stress, taken positive in compression; ρ_0 and ρ are the densities of target materials in the undeformed and deformed states; u and v are the displacement and particle velocity in the radial direction, with outward motion considered positive. Particle velocity and displacement are related by

$$v(1-\partial u/\partial r)=\partial u/\partial t \tag{2}$$

2.2 Equations of Material Mechanical Property

For a bilinear strain-hardening material, the uniaxial true stress-true strain relationship is shown schematically in Fig. 2 where E_1 and E_2 are the elastic and plastic moduli, respectively and Y is the yield stress. The uniaxial stress-strain relationship can be written as (setting $k=(1-\frac{E_2}{E_1})$ for simplification)

$$\sigma=E_1\varepsilon \qquad \sigma\leqslant Y \tag{3a}$$

$$\sigma=E_2\varepsilon+kY \qquad \sigma>Y \tag{3b}$$

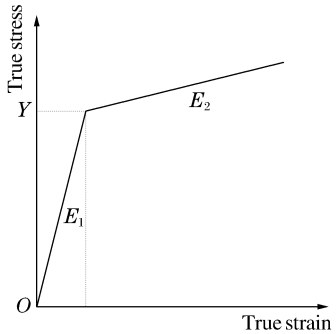


Fig. 2 Schematic diagram of stress-strain relationship for bilinear strain-hardening materials

The cylindrical cavity expansion problems are assumed as plane-strain, so $\varepsilon_z=0$. ε_r and ε_θ are defined as logarithmic strain components in radial and circumferential direction, respectively. The logarithmic strain-displacement relationship is

$$\varepsilon_r = \ln(1 - \partial u/\partial r) \tag{4a}$$

$$\varepsilon_\theta = \ln(1 - u/r) \tag{4b}$$

As the assumption of Bishop et al[1], the octahedral shear stress τ_n is a definite function of the octahedral shear strain γ_n for all strain states. In the case of uniaxial stress state

$$\tau_n = \sqrt{2}\sigma/3 \tag{5a}$$

$$\gamma_n = \frac{2\sqrt{2}}{3}(1+\nu)\varepsilon \tag{5b}$$

where ν is Poisson's ratio and for incompressible materials $\nu = 1/2$.

Substituting Eqs. (5a) and (5b) into Eq. (3b), then

$$\tau_n = \frac{E_2}{(1+\nu)}\gamma_n + \frac{\sqrt{2}}{3}kY \tag{6}$$

Following Hill[11], we assume that in plastic region the axial stress is equal to the average radial and circumferential stresses, or

$$\sigma_z = (\sigma_r + \sigma_\theta)/2 \tag{7}$$

where σ_r, σ_θ are the radial and circumferential components of Cauchy stress taken positive in compression.

For incompressible materials, $\varepsilon_r + \varepsilon_\theta = 0$, then

$$\tau_n = \frac{\sqrt{6}}{6}(\sigma_r - \sigma_\theta) \tag{8a}$$

$$\gamma_n = \frac{2\sqrt{6}}{3}\varepsilon_r \tag{8b}$$

For compressible materials,

$$\gamma_n = \frac{2}{3}\sqrt{\varepsilon_r^2 + \varepsilon_\theta^2 + (\varepsilon_r - \varepsilon_\theta)^2} \tag{8c}$$

Therefore, plastic flow for the cavity expansion problem is governed by Eq. (9a) for incompressible materials and Eq. (9b) for compressible materials as follows

$$\sigma_r - \sigma_\theta = \frac{4}{3}E_2\varepsilon_r + \frac{2\sqrt{3}}{3}kY \tag{9a}$$

$$\sigma_r - \sigma_\theta = \frac{2\sqrt{3}E_2}{3(1+\nu)}(\varepsilon_r^2 + \varepsilon_\theta^2 - \varepsilon_r\varepsilon_\theta)^2 + \frac{2\sqrt{3}}{3}kY \tag{9b}$$

Material compressibility is models by a linear pressure-volume relation. That is

$$p = (\sigma_r + \sigma_\theta + \sigma_z)/3 = K(1 - \rho_0/\rho) \tag{10}$$

where ρ, ρ_0 are the initial and current densities, K is the bulk modulus and p is the pressure.

2.3 Boundary Conditions

The plastic and elastic regions of response are linked through the Hugoniot jump condition that conserves mass and momentum across the elastic-plastic interface (where, $r = ct$)

$$\rho_2(c - v_2) = \rho_1(c - v_1) \tag{11a}$$

$$\rho_2 v_2(c - v_2) - \rho_1 v_1(c - v_1) = \sigma_{r2} - \sigma_{r1} \tag{11b}$$

where the subscripts 1, 2 denote the variables in elastic and plastic regions. It is obvious that for incompressible materials the velocity and radial stress are both continuous. On both sides of the interface between elastic and plastic regions, the von-Mises yield condition must be satisfied, viz.

$$\sigma_{r2} - \sigma_{\theta 2} = 2\sqrt{3}Y/3 \tag{12a}$$

$$\sigma_{r1} - \sigma_{\theta 1} = 2\sqrt{3}Y/3 \tag{12b}$$

On the elastic interface

$$p=\nu(\sigma_r+\sigma_\theta) \tag{13}$$

Combining Eqs. (11a), (11b), (12a), (12b), (13) and (10) and eliminating ρ_1, ρ_2, v_2, σ_2 can be denoted in terms of v_1, σ_1, which is shown in section 2.5 in forms of dimensionless variables.

Furthermore, the boundary condition at the cavity surface is

$$u(r=v_c t)=v_c t \tag{14}$$

2.4 Incompressible Bilinear Strain-Hardening Materials

2.4.1 Plastic Region

We adopt the same similarity transformation as Crozier and Hunter[9], viz.

$$\xi=r/ct \tag{15}$$

and the dimensionless variables

$$S=\sigma_r/Y,\quad \bar{u}=u/ct,\quad U=v/c,\quad \gamma=v_c/c \tag{16}$$

Thus, with Eqs. (9a), (10), (15) and (16) control Eqs. (1a), (1b), (2), can be recast into

$$\frac{\mathrm{d}S}{\mathrm{d}\xi}+\frac{4E_2}{3Y}\cdot\frac{1}{\xi}\ln\left(1-\frac{\mathrm{d}\bar{u}}{\mathrm{d}\xi}\right)+\frac{2/\sqrt{3}}{\xi}k=\frac{\rho_0 c^2}{Y}(\xi-U)\frac{\mathrm{d}U}{\mathrm{d}\xi} \tag{17a}$$

$$\frac{\mathrm{d}}{\mathrm{d}\xi}(\xi-\bar{u})^2=2\xi^2 \tag{17b}$$

$$U\left(1-\frac{\mathrm{d}\bar{u}}{\mathrm{d}\xi}\right)=\bar{u}-\xi\frac{\mathrm{d}\bar{u}}{\mathrm{d}\xi} \tag{17c}$$

Boundary conditions for incompressible materials yield

$$\bar{u}(\xi=\gamma)=\gamma \tag{18a}$$

$$S(\xi=1)=S_1 \tag{18b}$$

$$U(\xi=1)=U_1 \tag{18c}$$

where S_1 denotes the dimensionless radial stress on elastic side of elastic-plastic interface. Substituting Eq. (18a) into Eq. (17b), gives

$$\bar{u}=\xi-(\xi^2-\gamma^2)^{1/2} \tag{19}$$

From Eq. (19), we get

$$U=\gamma^2/\xi \tag{20}$$

Combining Eqs. (17a), (18b), (18c), (19) and Eq. (20), we obtain

$$S(\xi)=S_1-\frac{2\sqrt{3}}{3}k\ln\xi+\frac{\rho_0 c^2}{2Y}\gamma^2\left(\gamma^2-2\ln\xi-\frac{\gamma^2}{\xi^2}\right)+\frac{4}{3}\frac{E_2}{Y}\int_\xi^1\frac{1}{x}\ln\frac{x}{(x^2-\gamma^2)^{1/2}}\mathrm{d}x \tag{21a}$$

The integration term in Eq. (21a) can be rewritten as

$$\begin{aligned}\int_\xi^1\frac{1}{x}\ln\frac{x}{(x^2-\gamma^2)^{1/2}}\mathrm{d}x&=-\frac{1}{2}\int_\xi^1\frac{1}{x}\ln\left(1-\frac{\gamma^2}{x^3}\right)\mathrm{d}x=-\frac{1}{4}\int_{1-(\gamma/\xi)^2}^{1-\gamma^2}\frac{\ln x}{1-x}\mathrm{d}x=\\&-\frac{1}{4}\left(\int_{1-(\gamma/\xi)^2}^{1}\frac{\ln x}{1-x}\mathrm{d}x+\int_1^{1-\gamma^2}\frac{\ln x}{1-x}\mathrm{d}x\right)=\\&-\frac{1}{4}\left\{\mathrm{dilog}(1-\gamma^2)-\mathrm{dilog}\left[1-\left(\frac{\gamma}{\xi}\right)^2\right]\right\}\end{aligned} \tag{21b}$$

where the dilogarithmatic function is defined as follows

$$\mathrm{dilog}(x)=\int_1^x\frac{\ln t}{1-t}\mathrm{d}t \tag{21c}$$

2.4.2 Elastic Region

For the elastic region, the deformation is small. Then, the second order infinitesimal terms can be neglected. Thus, the mass conversation equation yields

$$\frac{\mathrm{d}\bar{u}}{\mathrm{d}\xi}+\frac{1}{\xi}\bar{u}=0 \tag{22}$$

Integrating Eq. (22) and rearranging give,

$$\bar{u} = D \cdot \frac{1}{\xi} \tag{23}$$

Similarly, the displacement-velocity relationship is

$$U = \bar{u} - \xi \frac{\mathrm{d}\bar{u}}{\mathrm{d}\xi} \tag{24a}$$

or

$$U = 2D \cdot \frac{1}{\xi} \tag{24b}$$

In elastic region, we have

$$\sigma_r - \sigma_\theta = \frac{E_1}{1+\nu}(\varepsilon_\theta - \varepsilon_r) \tag{25}$$

On the elastic-plastic boundary, using the condition $\xi = 1$ together with the von-Mises yield criterion, viz. $\sigma_r - \sigma_\theta = 2\sqrt{3}Y/3$, we obtain

$$D = \frac{\sqrt{3}Y}{2E_1} \tag{26}$$

The momentum conversation equation can be rewritten as

$$\frac{\mathrm{d}S}{\mathrm{d}\xi} + \frac{2E_1}{3Y} \cdot \frac{1}{\xi}\left(\frac{\bar{u}}{\xi} - \frac{\mathrm{d}\bar{u}}{\mathrm{d}\xi}\right) = -\frac{\rho_0 c^2}{Y}\xi^2 \frac{\mathrm{d}^2\bar{u}}{\mathrm{d}\xi^2} \tag{27}$$

At the infinite boundary, S must be of finite value. Thus

$$S(\xi) = \frac{\sqrt{3}}{3\xi^2} - \frac{\sqrt{3}\rho_0 c^2}{E_1}\ln\xi \tag{28a}$$

along with $\xi = 1$ at the elastic-plastic interface, one obtains

$$S_1 = \frac{2\sqrt{3}}{3} \tag{28b}$$

2.4.3 Response Equations

At the elastic-plastic interface ($\xi = 1$), the continuity condition $U_2 = U_1$ must be satisfied. Hence

$$\gamma = (2D)^{1/2} \tag{29a}$$

$$c = v_c/\gamma = v_c(E_1/\sqrt{3}Y)^{1/2} \tag{29b}$$

Substituting Eq. (28b) and Eq. (29b) into Eq. (21) the stress at the cavity can be written as

$$S(\xi = \gamma) = \frac{2\sqrt{3}}{3} - \frac{2\sqrt{3}}{3}k\ln\gamma + \frac{E_2}{3Y}[\mathrm{dilog}(0) - \mathrm{dilog}(1-\gamma^2)] + \frac{\rho_0 v_c^2}{Y}\left(\frac{\sqrt{3}Y}{2E_1} - \frac{1}{2} - \ln\gamma\right) \tag{30a}$$

or

$$\sigma_{r0}/Y = A + B[(\rho_0/Y)^{1/2}v_c]^2 \tag{30b}$$

where σ_{r0} represents stress at the cavity surface and A, B are evaluated by the following expressions

$$A = \frac{\sqrt{3}}{3}\left\{2 - k\ln\frac{\sqrt{3}Y}{E_1} + \frac{E_2}{\sqrt{3}Y}\left[\mathrm{dilog}(0) - \mathrm{dilog}\left(1 - \frac{\sqrt{3}Y}{E_1}\right)\right]\right\} \tag{31a}$$

$$B = \frac{1}{2}\left(\frac{\sqrt{3}Y}{E_1} - 1 - \ln\frac{\sqrt{3}Y}{E_1}\right) \tag{31b}$$

2.5 Compressible Bilinear Strain-Hardening Materials

2.5.1 Plastic Equations

For the compressible bilinear strain-hardening materials, the density ρ is no longer a constant, which means that the plastic wave velocity is also no longer a linear function of cavity expansion velocity and the compressibility equation must be taken into consideration. By Eq. (15), Eq. (16), Eqs. (1a), (1b), and Eq. (9b) can be recast into

$$\frac{\mathrm{d}S}{\mathrm{d}\xi}+\frac{E_2}{Y}\frac{1}{\xi}f\left(\xi,w,\frac{\mathrm{d}w}{\mathrm{d}\xi}\right)+\frac{1}{\xi}\frac{2\sqrt{3}}{3}k=\frac{\rho_0 c^2}{Y}\frac{w^3}{\xi}\frac{\mathrm{d}^2w/\mathrm{d}\xi^2}{(\mathrm{d}w/\mathrm{d}\xi)^2} \tag{32a}$$

$$S=\frac{1}{2}\frac{E_2}{Y}f\left(\xi,w,\frac{\mathrm{d}w}{\mathrm{d}\xi}\right)+\frac{K}{Y}\ln\left(\frac{\mathrm{d}w}{\mathrm{d}\xi}\frac{w}{\xi}\right)+\frac{\sqrt{3}}{3}k \tag{32b}$$

where

$$f\left(\xi,w,\frac{\mathrm{d}w}{\mathrm{d}\xi}\right)=\frac{2\sqrt{3}}{3(1+\nu)}\left(\ln^2\frac{\mathrm{d}w}{\mathrm{d}\xi}+\ln^2\frac{w}{\xi}-\ln\frac{\mathrm{d}w}{\mathrm{d}\xi}\ln\frac{w}{\xi}\right)^{1/2} \tag{32c}$$

$$w=\xi-\bar{u} \tag{32d}$$

On the plastic side interface, velocity, stress and yield criterion produces

$$S(\xi=1)=S_2 \tag{33a}$$

$$w(\xi=1)=(1-U_2)\left.\frac{\mathrm{d}w}{\mathrm{d}\xi}\right|_{\xi=1} \tag{33b}$$

$$\left.f\left(\xi,w,\frac{\mathrm{d}w}{\mathrm{d}\xi}\right)\right|_{\xi=1}=\frac{2\sqrt{3}}{3}k\frac{Y}{E_2} \tag{33c}$$

Eq. (14) can be rewritten as

$$w(\xi=\gamma)=0 \tag{33d}$$

The interface condition is obtained in Section 2.3, viz.

$$U_2=U_1+\frac{(1-2\nu)(S_1-1/\sqrt{3})}{3(K/Y-\rho_0 c^2/Y)} \tag{33e}$$

$$S_2=S_1+\frac{\rho_0 c^2}{3(K-\rho_0 c^2)}(1-2\nu)(S_1-1/\sqrt{3}) \tag{33f}$$

where U_1, S_1 will be given in the following section. Obviously, above equations can only be solved numerically.

2.5.2 Elastic Equations

The strain can be seen as a first order infinitesimal. Then the control equation can be obtained by neglecting the nonlinear items of the second order infinitesimal, viz.

$$\frac{E_1(1-\nu)}{(1+\nu)(1-2\nu)}\left(\frac{\partial^2 u}{\partial r^2}+\frac{1}{r}\frac{\partial u}{\partial r}-\frac{u^2}{r^2}\right)=\rho_0\frac{\partial^2 u}{\partial t^2} \tag{34}$$

The elastic wave velocity is defined as

$$c_{\mathrm{d}}^2=\frac{E_1(1-\nu)}{(1+\nu)(1-2\nu)\rho_0} \tag{35}$$

Eq. (34) can be rewritten into the following forms with the similarity transformation and dimensionless variables, i. e.

$$(1-\alpha^2\xi^2)\frac{\mathrm{d}^2\bar{u}}{\mathrm{d}\xi^2}+\frac{1}{\xi}\frac{\mathrm{d}\bar{u}}{\mathrm{d}\xi}-\frac{1}{\xi^2}\bar{u}=0 \tag{36a}$$

or

$$\bar{u}=C\left(\frac{\sqrt{1-\alpha^2\xi^2}}{\alpha\xi}-\alpha\xi\ln\frac{1+\sqrt{1-\alpha^2\xi^2}}{\alpha\xi}\right)+D\xi \tag{36b}$$

where C and D are constants to be determined and

$$\alpha=c/c_{\mathrm{d}} \tag{36c}$$

The boundary conditions are

$$\bar{u}(\xi=1/\alpha)=0 \tag{37a}$$

$$\sigma_{r1}-\sigma_{\theta 1}=2Y/\sqrt{3} \tag{37b}$$

Therefore, C and D can be evaluated through Eqs. (36a), (36b), (36c), (37a), (37b), constitutive equation and strain-stress relations in elastic region. Thus

$$\bar{u}=\frac{\sqrt{3}}{3}(1+\nu)\ \frac{Y}{E_1}\ \frac{\alpha}{\sqrt{1-\alpha^2}}\left(\frac{\sqrt{1-\alpha^2\xi^2}}{\alpha\xi}-\alpha\xi\ln\frac{\sqrt{1-\alpha^2\xi^2}}{\alpha\xi}\right) \tag{38a}$$

$$U=\bar{u}-\xi\frac{\mathrm{d}\bar{u}}{\mathrm{d}\xi}=\frac{2\sqrt{3}}{3}(1+\nu)\ \frac{Y}{E_1}\ \frac{\sqrt{1-\alpha^2\xi^2}}{\sqrt{1-\alpha^2}\,\xi} \tag{38b}$$

$$S=\frac{\sqrt{3}}{3}\ \frac{\alpha^2}{(1-2\nu)\ \sqrt{1-\alpha^2}}\left[(1-2\nu)\ \frac{\sqrt{1-\alpha^2\xi^2}}{\alpha^2\xi^2}+\ln\frac{1+\sqrt{1-\alpha^2\xi^2}}{\alpha\xi}\right] \tag{38c}$$

The velocity and stress solutions at the elastic-plastic interface are given by Eqs. (38b), (38c), viz.

$$U_1=\frac{2\sqrt{3}}{3}\ \frac{(1+\nu)Y}{E_1} \tag{39a}$$

$$S_1=\frac{\sqrt{3}}{3}\ \frac{\alpha^2}{(1-2\nu)\ \sqrt{1-\alpha^2}}\left[(1-2\nu)\ \frac{\sqrt{1-\alpha^2}}{\alpha^2}+\ln\frac{1+\sqrt{1-\alpha^2}}{\alpha}\right] \tag{39b}$$

2.5.3 Numerical Calculation

In plastic region, Eqs. (32a), (32b) contain the unknown physical quantities, S, w, $(\mathrm{d}w/\mathrm{d}\xi)c$, γ. Therefore, to solve the variables S, w, $\mathrm{d}w/\mathrm{d}\xi$ we must first set a value for c, and then calculation starts backward from the elastic-plastic interface $\xi=1$. When $w=0$, γ is known, and the expansion velocity $v_c=\gamma c$ can also be computed. The calculated v_c is compared with the actual expansion velocity and a loop of calculation is carried out with calculated of last step until the precision is satisfied.

For convenience, we differentiate Eq. (32b) and make the replacement

$$y_1(\xi)=S(\xi),\quad y_2(\xi)=w(\xi),\quad y_3(\xi)=w'(\xi) \tag{40}$$

Then, a system of differential equations is deduced from Eqs. (32a), (32b) and (40), Viz.

$$y'_1+H_1y'_3=H_2 \tag{41a}$$

$$y'_1+Q_1y'_3=Q_2 \tag{41b}$$

$$y'_2=y_3 \tag{41c}$$

Where

$$H_1=-\frac{\rho_0c^2}{Y}\ \frac{y_2^3}{\xi\cdot y_3^2} \tag{42a}$$

$$H_2=-\frac{1}{\xi}\left[\frac{2\sqrt{3}}{3}k+\frac{E_2}{Y}f(\xi,y_2,y_3)\right] \tag{42b}$$

$$Q_1=-\frac{1}{y_3}\left[\frac{E_2}{Y}\ \frac{2\ln y_3-\ln(y_2/\xi)}{3(1+\nu)^2f(\xi,y_2,y_3)}+\frac{K}{Y}\right] \tag{42c}$$

$$Q_2=\left(\frac{y_3}{y_2}-\frac{1}{\xi}\right)\left[\frac{E_2}{Y}\ \frac{-\ln y_3+2\ln(y_2/\xi)}{3(1+\nu)^2f(\xi,y_2,y_3)}+\frac{K}{Y}\right] \tag{42d}$$

Then

$$y'_1=(H_2Q_1-H_1Q_2)/(Q_1-H_1) \tag{43a}$$

$$y'_2=y_3 \tag{43b}$$

$$y'_3=(Q_2-H_2)/(Q_1-H_1) \tag{43c}$$

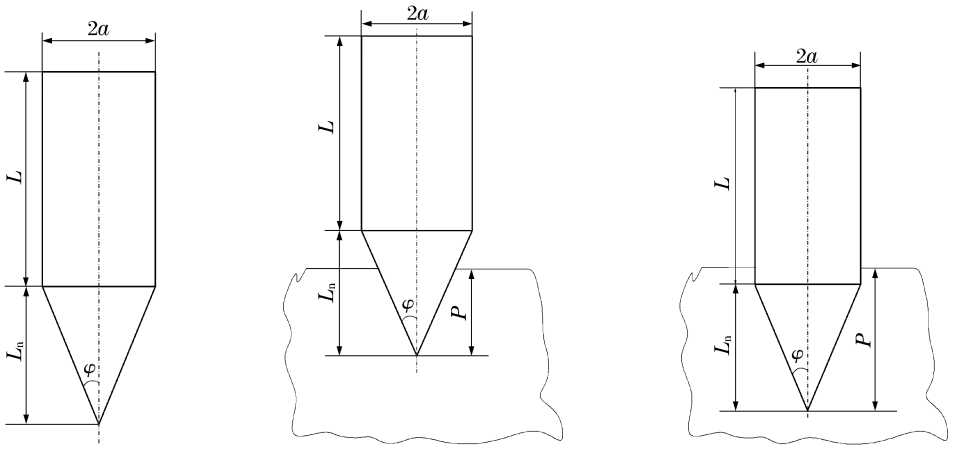
The initial conditions at boundary $\xi=1$ for y_1, y_2, y_3 can be given by Eqs. (33b), (33c), (33f).

We developed Adams-Bashforth finite difference codes to carry on the calculation. It is robust although it will encounter the difficulty as those discussed by Luk et al[6]. The integrator can monitor y'_3 and adjust the integration step in case that it becomes too large as $y_2\to 0$.

3 Penetration Equations

We consider the penetration of ductile metal targets subjected to impact by conical-nosed projectiles. The geometry of conical-nosed projectiles is shown schematically in Fig. 3(a). Two situations

may arise considering the penetration of the projectile impacting on semi-infinite targets as shown schematically in Fig. 3(b) and Fig. 3(c). One is that the final depth of penetration has not reached the shoulder of the projectiles as shown in Fig. 4(b), and the other is that the final depth of penetration is larger than the nose length L_n as shown in Fig. 3(c)[12-14].



(a) Geometry (b) Impacting when $P \leqslant L_n$ (c) Impacting when $P > L_n$

Fig. 3 Schematic diagram of a conical-nosed projectile

From the projectile geometry, the radial velocity, v_r, at the nose interface can be expressed as

$$v_r = v_z \tan\varphi \tag{44a}$$

where, v_z is the projectile impact velocity and φ is defined as in Fig. 3(a).

As discussed by Forrestal[16], we can assume that during penetration a film of melted target material is formed between the nose and target. Thus, penetration resistance is assumed to consist of stresses normal to the nose and a tangential, frictional component. We assume the tangential stress on the nose σ_t is proportional to the normal stress σ_n

$$\sigma_t = \mu\sigma_r \tag{44b}$$

As for the frictional coefficient, μ, Bowden and Tabor[17] found experimentally that values of μ were velocity dependent and varied between $\mu = 0.10 \sim 0.20$. Montgomery[18] measured sliding frictional resistance on projectile rotating bands during field test of gun launches and suggests a frictional coefficient of $\mu = 0.02$ at high-velocity. In the following section, we consider a set of values of μ to select the most suitable μ in the calculation.

For the present penetration problem, we can approximate that

$$\sigma_r = \sigma_{r0}(v_z) \tag{44c}$$

where σ_{r0} is the radial stress on the cavity surface, which can be deduced σ_{r0} is determined by Eq. (30b) and the coefficients A, B are given by Eqs. (31a), (31b) for incompressible models and by curve-fitting from the numerical results of stress on the cavity surface versus impact velocities for compressible model.

3.1 Case Ⅰ $P \leqslant L_n$

Defining z as the position of nose in the penetration direction at a moment, the force acting on the projectile nose in the penetration direction (axial direction) is

$$F_z = \pi z^2 \tan\varphi(\mu + \tan\varphi)(AY + B\rho_0 v_z^2 \cdot \tan^2\varphi) \tag{45a}$$

Using Newton's second law of motion, we obtain

$$m\frac{\mathrm{d}v_z}{\mathrm{d}t} = mv_z\frac{\mathrm{d}v_z}{\mathrm{d}z} = -F_z \tag{45b}$$

Or

$$\frac{mv_z\mathrm{d}v_z}{AY+B\rho_0 v_z^2\tan^2\varphi}=-\pi\tan\varphi(\mu+\tan\varphi)z^2\mathrm{d}z \tag{45c}$$

Integrating Eq. (44c) yields the expression for the depth of penetration

$$P=\left[\frac{3m\ln\left(1+\dfrac{B}{A}\dfrac{\rho_0 v_0^2}{Y}\tan^2\varphi\right)}{2\pi B\rho_0\tan^3\varphi(\mu+\tan\varphi)}\right]^{1/3} \tag{45d}$$

3.2 Case Ⅱ　$P>L_n$

In this case, the nose of projectile is completely embedded in the target. Therefore, the force acting on the projectile nose in the penetration direction (axial direction) can now be expressed as

$$F_z=\pi a^2(1+\mu/\tan\varphi)(AY+B\rho_0 v_z^2\tan^2\varphi) \tag{46a}$$

Substituting Eq. (45a) into Eq. (44b) and integrating it, we obtain

$$P=\frac{a}{\tan\varphi}+\frac{m\ln\left(1+\dfrac{B}{A}\dfrac{\tilde{v}_0^2}{Y}\tan^2\varphi\right)}{2\pi B\rho_0 a^2\tan\varphi(\mu+\tan\varphi)} \tag{46b}$$

where $\tilde{v}_0$ denoting the residual velocity after the situation of Case Ⅰ. Integrating Eq. (45c) yields

$$\frac{m}{2\pi B\rho_0\tan^3\varphi(\mu+\tan\varphi)}\left[\ln\left(1+\frac{B}{A}\frac{\rho_0\tilde{v}_0}{Y}\tan^2\varphi\right)-\ln\left(1+\frac{B}{A}\frac{\rho_0 v_0}{Y}\tan^2\varphi\right)\right]=\frac{1}{3}L_n^3 \tag{46c}$$

Therefore, Eq. (46b) is rewritten as

$$P=\frac{2a}{3\tan\varphi}+\frac{m\ln\left(1+\dfrac{B}{A}\dfrac{v_0^2}{Y}\tan^2\varphi\right)}{2\pi B\rho_0 a^2\tan\varphi(\mu+\tan\varphi)} \tag{46d}$$

4 Results and Discussion

We applied the above models to the 6060-T651 Alaluminum alloy material. Fig. 4 shows the experimental true stress versus true strain graph of the material, which was reported in Ref. [4]. A bilinear model with $Y=317$ MPa, $E_2=63$ MPa provides the best fit to the data as shown in Fig. 4. For comparison, a power law fit with $n=0.051$ adopted by Luk et al.[7] is also presented in Fig. 4.

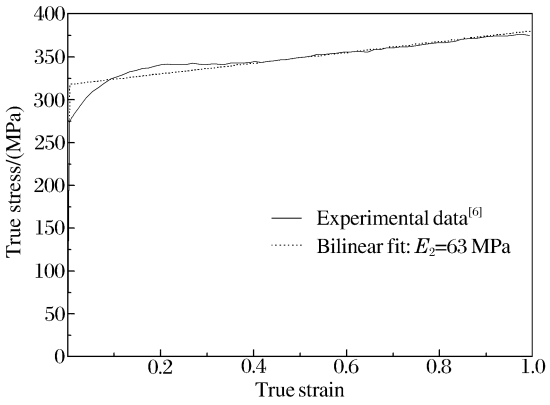


Fig. 4　Experimental true stress-strain curve and the bilinear and power-law data-fit for 6061-T651

4.1 Cavity Expansion

The elastic-plastic interface velocities c versus the cavity expansion v_c velocity are shown in Fig. 5. The interface velocities for the incompressible bilinear strain-hardening model are given by Eq. (30b) and are computed numerically for the compressible bilinear strain-hardening model. In the case of lower velocity, the results between incompressible and compressible models are negligibly small. With the increase of cavity expansion velocity v_c, the compressibility effect becomes more important, which results in the big difference between the incompressible and compressible models as can be seen from Fig. 5. The results of the bilinear models with $E_2=0$, 500 MPa are also presented in Fig. 5. It can be seen from Eq. (29) that strain hardening has no effects on the relationship between the elastic-plastic interface velocity and the cavity expansion velocity for incompressible model. Similar conclusion can be drawn for compressible model as can be seen from Fig. 5.

Fig. 6 shows the radial stress distribution when $v_c = 400$ m/s. It is seen that the effect of strain hardening is small and completely diminishes with distance. The difference between incompressible and compressible models is also not so big. There is a small discontinuity in radial stress at the plastic-elastic interface for the compressible models, while it is continuous for incompressible models.

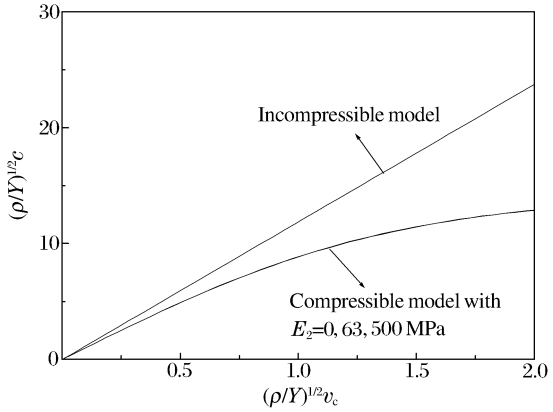


Fig. 5 Elastic-plastic interface velocity versus cavity expansion velocity

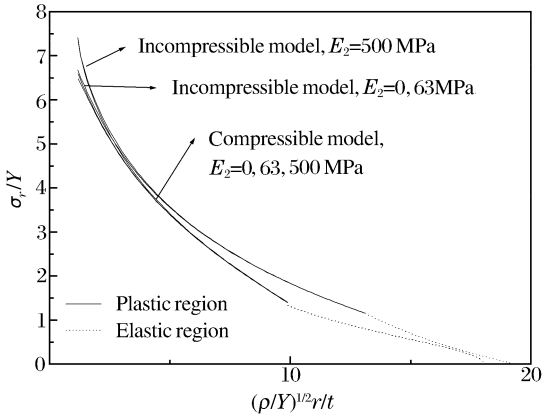


Fig. 6 Radial stress distribution for $v_c = 400$ m/s

Fig. 7 shows the graphs of stress on cavity surface versus cavity expansion velocity, which is compared between incompressible and compressible models with different plastic moduli. It can be seen that the effect of compressibility is small, whereas the effect of strain hardening is relatively great which makes much difference for models with $E_2 = 500$ MPa compared to those with $E_2 = 0$, 63 MPa.

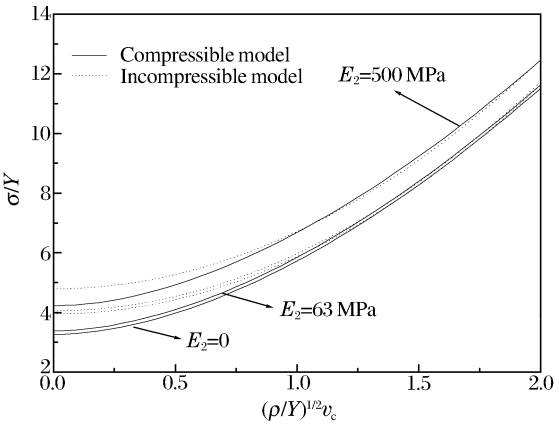


Fig. 7 Radial stress on the cavity surface versus the expansion velocity for bilinear model

4.2 Penetration

The coefficients A and B in Eqs. (44d), (45b) for all the models considered above are listed in Table 1. The predicted depths of penetration are then compared with the experimental data for the 6061-T651 aluminum alloy targets subjected to impact by 7.1 mm diameter conical-nosed rods[15].

Table 1 Coefficients for the expressions of stress on the cavity surface in different models

E_2/(MPa)	Incompressible		Compressible	
	A	B	A	B
0	3.945	1.920	3.492	2.075
63	4.050	1.920	3.613	2.073
500	4.785	1.920	4.447	2.074

Fig. 8 shows comparisons between experimental data for conical nosed rods and the prediction of compressible bilinear strain-hardening model with $E_2 = 63$ MPa when $\mu = 0.05, 0.10, 0.15, 0.20$. It can be seen that the predictions are very sensitive to μ and $\mu = 0.15$ gives the best fit to experiments.

Further to clarify the influence of compressibility and strain-hardening on depth of penetration for bilinear models, Fig. 9 presents the results predicted by the incompressible and compressible bilinear

models with different plastic moduli E_2. It is evident for Fig. 9 that the influence of compressibility is negligibly small. However, the effect of plastic modulus on penetration is relatively significant. The larger the plastic modulus is, the smaller the depth of penetration is.

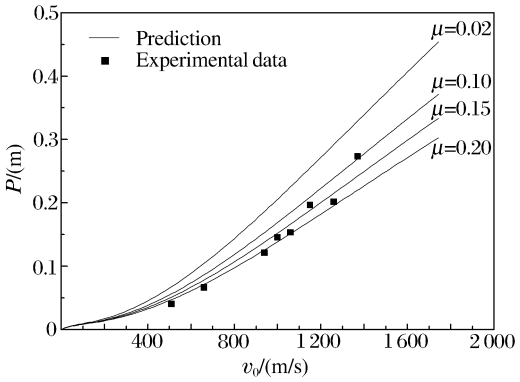


Fig. 8　Predictions of DOP under different values of μ

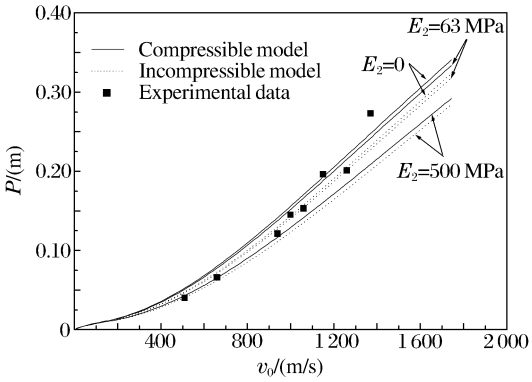


Fig. 9　Predictions of DOP of different models for 6061-T651 Al materials under impact of ogival-nosed rods

5　Conclusions

A theoretical study has been given herein on dynamic expansion of cylindrical cavity from zero initial radius and its application to penetration problems. Both incompressible and compressible bilinear strain-hardening materials are considered. Solutions for dynamic cylindrical cavity expansion are obtained in terms of the velocity of plastic wave front, radial stress distribution and stress on the cavity surface. The influence of material properties, such as compressibility, elastic-plastic constitutive equations and plastic modulus is then discussed. Based on the models, penetration equations are then constructed. Comparison with experimental data and the existing power law models is made. It shows that the present theoretical predictions are in good agreement with experimental observations.

It is shown that the compressibility has negligible effect on radial stress distribution and stress on the cavity surface etc., whereas the effect of strain-hardening is relatively significant.

For the corresponding penetration problems, it is found that the predictions by various models with $\mu=0.15$ are in good agreement with the available experimental data for 6061-T651 aluminum targets. It is also found that the influence of plastic modulus for bilinear stain-hardening materials is significant for the prediction of penetration depth especially at higher impact velocities.

References:

[1] Bishop R F, Hill R, Mott N F. The Theory of Indentation and Hardness Tests [J]. Proceeding of the Physical Society, 1948, 57: 147-159.

[2] Wright S C, Huang Y, Fleck N A. Deep Penetration of Polycarbonate by a Cylindrical Punch [J]. Mech Mater, 1992, 13: 277-284.

[3] Satapathy S, Bless S J. Deep Punching PMMA [J]. Exp Mech, 2000, 40(1): 31-38.

[4] Goodier J N. On the Mechanics of Indentation and Cratering in Solid Targets of Strain-Hardening Metal by Impact of Hard and Soft Sphere [A]. //Proceedings of the 7th Symp Hypervelocity Impact, Vol. Ⅲ [C]. [s. l.] AIAA, J, 1965.

[5] Forrestal M J. Penetration into Dry Porous Rock [J]. Int J Solids Struct, 1986, 22(12): 1485-1500.

[6] Luk V K, Forrestal M J, Amos D E. Dynamic Spherical Cavity Expansion of Strain-Hardening Materials [J]. J Ap-

pl Mech,1991,58:1-6.

[7] Luk V K, Amos D E. Dynamic Cylindrical Cavity Expansion of Compressible Strain-Hardening Materials [J]. J Appl Mech,1991,58:334-340.

[8] Forrestal M J, Tzou D Y. A Spherical Cavity-Expansion Penetration Model for Concrete Targets [J]. Int J Solids Struct,1997,34(31-32):4127-4146.

[9] Crozier R J M, Hunter S C. Similarity Solution for the Rapid Uniform Expansion of a Cylindrical Cavity in a Compressible Elastic-Plastic Solid [J]. Quarterly J Mech & Appl Math,1969,21:349-363.

[10] Longcope D B, Forrestal M J. Penetration of Targets Described by a Mohr-Coulomb Failure Criterion with a Tension Cutoff [J]. J Appl Mech,1983,50:327-333.

[11] Hill R. General Features of Plastic-Elastic Problems as Exemplified by Some Particular Solutions [J]. ASME J Appl Mech,1949,16:295-300.

[12] Wen H M. Predicting the Penetration and Perforation of FRP Laminates Struck Normally by Projectiles with Different Nose Shapes [J]. Composite Structures,2000,49(3):321-329.

[13] Wen H M. Penetration and Perforation of Thick FRP Laminates [J]. Composites Science and Technology,2001,61(8):1163-1172.

[14] Wen H M. Predicting the Penetration and Perforation of Targets Struck by Projectiles at Normal Incidence [J]. Mech Structures & Machines,2002,30(4):543-577.

[15] Forrestal M J, Okajima K, Luk V K. Penetration of 6061-T651 Aluminum Targets with Rigid Long Rods [J]. ASME J Appl Mech,1988,55(4):755-760.

[16] Forrestal M J, Brar N S, Luk V K. Penetration of Strain-Hardening Targets With Rigid Spherical-Nose Rodes [J]. ASME J Appl Mech,1991,58:7-10.

[17] Bowden F P, Tabor D. The Friction and Lubrication of Solid, Part 2 [M]. London: Oxford University Press,1968: Chap 22.

[18] Montgomery R S. Surface Melting of Rotating Bands [J]. Wear,1976,38:235-243.

动态柱形空穴膨胀模型及其在侵彻问题中的应用

周 辉,文鹤鸣

(中国科技大学力学和机械工程系,安徽合肥 230027)

摘要:对双线性应变强化材料的动态柱形空穴膨胀模型及其在侵彻问题中的应用进行了研究。通过采用相似变换求解塑性区控制方程,获得了动态柱形空穴膨胀中的弹塑性界面速度、径向应力分布、空穴表面应力的解。基于柱形空穴模型,推导了侵彻方程,并将其得到的预测结果与侵彻实验数据进行了比较。结果表明,模型的理论解与现有数据吻合得很好。结果还显示了材料的可压缩性和塑性强化模量对柱形空穴膨胀以及侵彻阻力的影响。

关键词:动态柱形空穴膨胀;双线性强化;材料性能;侵彻

中图分类号:O385 **文献标识码**:A